NASA Technical Memorandum 106203
ICOMP–93–14

Large Time-Step Stability of Explicit One-Dimensional Advection Schemes

B.P. Leonard
Institute for Computational Mechanics in Propulsion
Lewis Research Center
Cleveland, Ohio

and The University of Akron
Akron, Ohio

May 1993

NASA

LARGE TIME-STEP STABILITY OF EXPLICIT ONE-DIMENSIONAL ADVECTION SCHEMES

B.P. Leonard*
Institute for Computational Mechanics in Propulsion
Lewis Research Center
Cleveland, Ohio 44135

and The University of Akron
Akron, Ohio 44325

ABSTRACT

There is a wide-spread belief that most explicit one-dimensional advection schemes need to satisfy the so-called "CFL condition" — that the Courant number, $c = u\Delta t/\Delta x$, must be less than or equal to one, for stability in the von Neumann sense. This puts severe limitations on the time-step in high-speed, fine-grid calculations and is an impetus for the development of implicit schemes, which often require less restrictive time-step conditions for stability, but are more expensive per time-step. However, it turns out that, at least in one dimension, if explicit schemes are formulated in a consistent flux-based conservative finite-volume form, von Neumann stability analysis *does not place any restriction* on the allowable Courant number. Any explicit scheme that is stable for $c < 1$, with a complex amplitude ratio, $G(c)$, can be easily extended to arbitrarily large c. The complex amplitude ratio is then given by $\exp(-\imath N\theta)\ G(\Delta c)$, where N is the integer part of c, and $\Delta c = c - N\ (< 1)$; this is clearly stable. The CFL condition is, in fact, not a stability condition at all, but, rather, a "range restriction" on the "pieces" in a piece-wise polynomial interpolation. When a global view is taken of the interpolation, the need for a CFL condition evaporates. A number of well-known explicit advection schemes are considered and thus extended to large Δt. The analysis also includes a simple interpretation of (large-Δt) TVD constraints.

INTRODUCTION

Consider the model one-dimensional pure advection equation for a scalar $\phi(x,t)$

$$\frac{\partial \phi}{\partial t} = -u\,\frac{\partial \phi}{\partial x} \tag{1}$$

where u is a constant advecting velocity. Take a uniform space-time grid (Δx, Δt) and integrate Equation (1) over Δx and Δt, giving a *finite-volume* formulation

$$\bar{\phi}_i^{n+1} = \bar{\phi}_i^{n} - c\,(\phi_r - \phi_l) \tag{2}$$

where the bars indicate spatial averages over cell i at time-levels n and $(n+1)$, and left and

*Work funded under Space Act Agreement NCC 3-233.

right *time-averaged* face-values have been introduced. The Courant number is given by

$$c = u\Delta t/\Delta x \tag{3}$$

The notation is defined in Figure 1, which also shows advective characteristics (along any one of which ϕ is constant) entering the left face (for $u > 0$). Given the set of current spatial-average values, $\bar{\phi}_i^n$, one needs to estimate the corresponding time-averaged face-values in order to explicitly update according to Equation (2).

In a von Neumann stability analysis, $\phi(x,t)$ is written as a wave [Fletcher, 1990]

$$\phi(x,t) = A(t)\exp(\imath kx) \tag{4}$$

where k is the wave number and $\imath$ represents the imaginary unit, $\sqrt{-1}$. When this is substituted into Equation (1), the *exact* solution is [Leonard, 1980]

$$\phi(x,t) = A(0)\exp[\imath k(x-ut)] \tag{5}$$

corresponding to a travelling wave, with ϕ = const along characteristics ($x = ut$). The *exact* complex amplitude ratio is then

$$\mathbf{G}_{\text{exact}} = \frac{\phi(x,t+\Delta t)}{\phi(x,t)} = \exp(-\imath c\theta) \tag{6}$$

where θ is the nondimensional wave-number

$$\theta = k\Delta x \tag{7}$$

Note that if $c > 1$, $\mathbf{G}_{\text{exact}}$ can be written

$$\mathbf{G}_{\text{exact}} = \exp(-\imath N\theta)\,\exp(-\imath \Delta c\theta) \tag{8}$$

where N is the integer part of c

$$N = \text{INT}(c) \tag{9}$$

and Δc the non-integer part (necessarily less than one)

$$\Delta c = c - N \tag{10}$$

By integrating Equation (4) from $(x_i - \Delta x/2)$ to $(x_i + \Delta x/2)$, it is not difficult to show that the *exact* cell-average values are

$$\bar{\phi}_i^n = A(0)\,\exp\{\imath k[x_i - un\Delta t]\}\left(\frac{\sin\theta/2}{\theta/2}\right) \tag{11}$$

and

$$\bar{\phi}_i^{n+1} = A(0)\,\exp\{\imath k[x_i - u(n+1)\Delta t]\}\left(\frac{\sin\theta/2}{\theta/2}\right) \tag{12}$$

Hence, the *exact* complex amplitude ratio of cell-average values is the same as that given by Equation (8)

$$\bar{\mathbf{G}}_{\text{exact}} \;=\; \frac{\bar{\phi}_i^{n+1}}{\bar{\phi}_i^{n}} \;=\; \mathbf{G}_{\text{exact}} \;=\; \exp(-\iota N\theta)\,\exp(-\iota\,\Delta c\,\theta) \tag{13}$$

thus, giving a reference value against which to compare numerical G's.

In the following sections, the von Neumann stability of some well-known explicit advection schemes is studied — first in terms of the "conventional" time-step ranges, and then for larger Courant number values. The latter extension stems naturally from identifying the *sub-grid interpolation* used in estimating the time-averaged face-values in Equation (2). It will be shown, in particular, that if $\mathbf{G}_{\text{num}}^{\text{STS}}(c)$ is the (conventional, small time-step) complex amplitude ratio for a given scheme for $c \le 1$, then the natural finite-volume extension to arbitrarily large time-step has a complex amplitude ratio of the form

$$\mathbf{G}_{\text{num}}^{\text{LTS}}(c) \;=\; \frac{\bar{\phi}_i^{n+1}}{\bar{\phi}_i^{n}} \;=\; \exp(-\iota N\theta)\;\mathbf{G}_{\text{num}}^{\text{STS}}(\Delta c) \quad \text{for} \quad c > 1 \tag{14}$$

which should be compared with Equation (13). To the extent that $\mathbf{G}_{\text{num}}^{\text{STS}}(\Delta c)$ is a good approximation to $\exp(-\iota\,\Delta c\,\theta)$, then the large-$\Delta t$ $\mathbf{G}_{\text{num}}^{\text{LTS}}(c)$ is an even better approximation to the exact **G**. Viewed differently, a numerical simulation (over a given distance) will be more accurate for larger Δt because, as will become evident, numerical distortion depends only on the total number of time steps and Δc — not on c itself.

EXPLICIT ADVECTION SCHEMES

The time-averaged face-values appearing in Equation (2) can be rewritten in terms of spatial averages. For example, the time averaged left-face value is given by

$$\phi_t \;=\; \frac{1}{\Delta t}\int_0^{\Delta t} \hat{\phi}_t(\tau)\,d\tau \;=\; \frac{1}{c\Delta x}\int_{x_t - c\Delta x}^{x_t} \phi^n(\xi)\,d\xi \tag{15}$$

where $\hat{\phi}_t(\tau)$ is the instantaneous face-value and $\phi^n(\xi)$ is the local sub-grid spatial behaviour in the region upstream of the face in question, at time-level n. The relationship should be clear from Figure 1; note that $u\Delta t = c\Delta x$. A similar formula holds for the right face. But it is not necessary to write this out explicitly because advective flux *conservation* guarantees that

$$\phi_r(i) \;=\; \phi_t(i+1) \tag{16}$$

Different numerical schemes result from different choices of $\phi^n(\xi)$ in estimating the local behaviour. Note in particular that for consistency, $\phi^n(\xi)$ should obey the *integral constraint*

$$\frac{1}{\Delta x}\int_{x_i - \Delta x/2}^{x_i + \Delta x/2} \phi^n(\xi)\,d\xi \;=\; \bar{\phi}_i^n \qquad \text{for all } i \tag{17}$$

First-Order Upwinding

One of the simplest advection schemes results from assuming that $\phi^n(\xi)$ is piece-wise constant, for each i,

$$\phi^n(\xi) = \bar{\phi}_i^n \quad \text{for} \quad \left(x_i - \frac{\Delta x}{2}\right) < \xi < \left(x_i + \frac{\Delta x}{2}\right) \tag{18}$$

with discontinuities at the cell faces, as shown in Figure 2, the hatched region depicting the integral in Equation (15). This, of course, trivially satisfies Equation (17), and the left-face value given by Equation (15) for a positive Courant number *less than (or equal to) one* is simply

$$\phi_l(i) = \bar{\phi}_{i-1}^n \quad \text{for} \quad 0 < c \leq 1 \tag{19}$$

and, similarly

$$\phi_r(i) = \bar{\phi}_i^n \quad \text{for} \quad 0 < c \leq 1 \tag{20}$$

The update equation, Equation (2), thus becomes

$$\bar{\phi}_i^{n+1} = \bar{\phi}_i^n - c\,(\bar{\phi}_i^n - \bar{\phi}_{i-1}^n) \quad \text{for} \quad 0 < c \leq 1 \tag{21}$$

The corresponding complex amplitude ratio is

$$\mathbf{G}_{1U}(c) = 1 - c[1 - \exp(-\imath\,\theta)] \tag{22}$$

or

$$\mathbf{G}_{1U}(c) = 1 - c(1 - \cos\theta) - \imath\, c \sin\theta \tag{23}$$

For the full range of numerical wave-numbers ($0 \leq \theta \leq \pi$), this represents a semicircle of radius c in the lower half of the complex plane, passing through the point (1,0). The scheme is thus stable ($|\mathbf{G}| \leq 1$) *provided the CFL condition* ($c \leq 1$) *is satisfied.* Figure 3 shows a polar plot of $\mathbf{G}_{1U}$ for $c = 0.75$.

Making a Taylor expansion of real and imaginary parts gives

$$\mathbf{G}_{1U}(c) = 1 - \frac{c}{2}\,\theta^2 + O(\theta^4) - \imath\,[c\theta + O(\theta^3)] \tag{24}$$

whereas a Taylor expansion of the exact $\mathbf{G}$ gives

$$\begin{aligned} \mathbf{G}_{exact}(c) &= \cos(c\theta) - \imath\,\sin(c\theta) \\ &= 1 - \frac{c^2}{2}\,\theta^2 + O(\theta^4) - \imath\left[c\theta - \frac{c^3}{6}\,\theta^3 + O(\theta^5)\right] \end{aligned} \tag{25}$$

Thus $\mathbf{G}_{1U}$ indeed matches $\mathbf{G}_{exact}$ only through first-order terms in θ, with discrepancies in the second-order term (unless $c \equiv 1$, in which case exact cell-to-cell transfer occurs across one mesh-width: $\bar{\phi}_i^{n+1} = \bar{\phi}_{i-1}^n$).

Second-Order Methods

It is convenient to define the "order" of an advection scheme as the power of θ up to and including which the Taylor expansion of G_{num} matches that of G_{exact} given by Equation (25). One of the best known second-order methods is that due to Lax and Wendroff [1960], equivalent in the scalar case to Leith's method [1965]. For this scheme, the sub-grid $\phi^n(\xi)$ is assumed to be piece-wise linear satisfying Equation (17). Upstream of the left face, for example, a straight line is drawn (for $u > 0$) between $\bar{\phi}^n_{i-1}$ and $\bar{\phi}^n_i$, considered to be located at the centers of the respective finite-volume cells. A similar construction is made across each of the other cells, resulting in discontinuities at cell faces. This is shown in Figure 4, which also indicates the integral in Equation (15) for $0 < c < 1$.

In this case, i.e., for a Courant number *less than (or equal to) one*,

$$\phi^n(\xi) = \bar{\phi}^n_{i-1} + \left(\frac{\bar{\phi}^n_i - \bar{\phi}^n_{i-1}}{\Delta x}\right)(\xi - x_{i-1}) \quad \text{for} \quad \left(x_{i-1} - \frac{\Delta x}{2}\right) < \xi < \left(x_{i-1} + \frac{\Delta x}{2}\right) \tag{26}$$

upstream of the left face, across cell $(i-1)$. Substitution into Equation (15) results in

$$\phi_\ell(i) = \frac{1}{2}(\bar{\phi}^n_i + \bar{\phi}^n_{i-1}) - \frac{c}{2}(\bar{\phi}^n_i - \phi^n_{i-1}) \tag{27}$$

According to Equation (16), ϕ_r is obtained by increasing each index by 1. This gives the update equation as

$$\bar{\phi}^{n+1}_i = \bar{\phi}^n_i - \frac{c}{2}(\bar{\phi}_{i+1} - \bar{\phi}^n_{i-1}) + \frac{c^2}{2}(\bar{\phi}_{i+1} - 2\bar{\phi}_i + \bar{\phi}_{i-1}) \tag{28}$$

Because of the symmetry about cell i, this formula is actually valid for positive or negative Courant number, provided

$$|c| \leq 1 \tag{29}$$

The negative-c case is shown in Figure 5, where the sub-grid $\phi^n(\xi)$ for computing ϕ_ℓ is the same formula as that in Equation (26) — but across cell i rather than $(i-1)$.

The numerical complex amplitude ratio for the Lax-Wendroff scheme can be obtained directly from Equation (28) as

$$G_{LW}(c) = 1 - \frac{c}{2}[\exp(\iota\theta) - \exp(-\iota\theta)] + \frac{c^2}{2}[\exp(\iota\theta) - 2 + \exp(-\iota\theta)] \tag{30}$$

or

$$G_{LW}(c) = 1 - c^2(1 - \cos\theta) - \iota c \sin\theta \tag{31}$$

with a corresponding Taylor expansion

$$G_{LW}(c) = 1 - \frac{c^2}{2}\theta^2 + O(\theta^4) - \iota\left[c\theta - \frac{c}{6}\theta^3 + O(\theta^5)\right] \tag{32}$$

thus matching the expansion of G_{exact}, Equation (25), through θ^2 terms, as expected for a second-order scheme. Once again, exact point-to-point transfer across one mesh-width occurs when $c \equiv 1$ (and also, in this case, when $c \equiv -1$). Figure 6 shows a polar plot of G_{LW}, a semi-ellipse with vertical semi-axis equal to c and curvature near (1,0) equal to that of the unit circle. The scheme is stable *provided the CFL condition is satisfied* — and unstable otherwise.

The Lax-Wendroff scheme is symmetrical in the sense that a given face-value (assuming $|c| \leq 1$) depends only on the two immediately adjacent cell-average values on either side of the face in question. Figure 7 shows an alternate piece-wise linear sub-grid reconstruction (for positive c) using the two immediate *upstream* cell-average values. Although the reconstruction of $\phi^n(\xi)$ looks superficially the same as that in Figure 5, this represents an entirely different advection scheme in that the integral of Equation (15) is computed from the *left* (rather than the right, as in Figure 5). This will be found to generate a second-order advection scheme. Because of the upwind bias, it is now commonly known as "second-order upwinding" [Fletcher, 1990]. Upstream of the left face, across cell $(i-1)$, $\phi^n(\xi)$ is given by

$$\phi^n(\xi) = \bar{\phi}^n_{i-1} + \left(\frac{\bar{\phi}^n_{i-1} - \bar{\phi}^n_{i-2}}{\Delta x}\right)(\xi - x_{i-1}) \quad \text{for} \quad \left(x_{i-1} - \frac{\Delta x}{2}\right) < \xi < \left(x_{i-1} + \frac{\Delta x}{2}\right) \tag{33}$$

Equation (15) then gives the left-face value as

$$\phi_l = \left(\frac{3-c}{2}\right)\bar{\phi}_{i-1} - \left(\frac{1-c}{2}\right)\bar{\phi}_{i-2} \quad \text{for} \quad 0 < c \leq 1 \tag{34}$$

In fact, this equation is valid for $0 < c \leq 2$. This is an important point (usually ignored in CFD literature) because, as described below, it suggests a natural and computationally efficient way of extending explicit advection schemes to *arbitrarily large* Courant numbers.

Using the corresponding ϕ_r, the update equation for second-order upwinding becomes

$$\bar{\phi}^{n+1}_i = \bar{\phi}^n_i - c\left[\left(\frac{3-c}{2}\right)\bar{\phi}^n_i - (2-c)\,\bar{\phi}^n_{i-1} + \left(\frac{1-c}{2}\right)\bar{\phi}^n_{i-2}\right] \tag{35}$$

and the complex amplitude ratio is

$$G_{2U}(c) = 1 - c\left(\frac{3-c}{2}\right) + c\,(2-c)\cos\theta - c\left(\frac{1-c}{2}\right)\cos 2\theta$$
$$- \imath\left[c(2-c)\sin\theta - c\left(\frac{1-c}{2}\right)\sin 2\theta\right] \tag{36}$$

This has a Taylor expansion given by the following

$$G_{2U}(c) = 1 - \frac{c^2}{2}\theta^2 + O(\theta^4) - \iota\left[c\theta - \left(\frac{3c^2-2c}{6}\right)\theta^3 + O(\theta^5)\right] \tag{37}$$

Note in particular that, for $c \equiv 1$,

$$G_{2U}(1) = \cos\theta - \iota\sin\theta = G_{exact}(1) \tag{38}$$

corresponding to exact cell-to-cell transfer across one mesh-width. But, in addition, note that for $c \equiv 2$,

$$G_{2U}(2) = \cos 2\theta - \iota\sin 2\theta = G_{exact}(2) \tag{39}$$

with exact cell-to-cell transfer across *two* mesh-widths. In fact, second-order upwinding is stable throughout the entire range

$$|G_{2U}| \le 1 \quad \text{for} \quad 0 \le c \le 2 \tag{40}$$

Two typical polar plots (for $c = 0.75$ and 1.75) are shown in Figures 8 and 9, respectively.

In order to prove (40), it is convenient to rewrite $G_{2U}(c)$ in the following form, starting with Equation (36),

$$G_{2U}(c) = (\cos\theta - \iota\sin\theta)\left[1 - (c-1)^2(1-\cos\theta) - \iota(c-1)\sin\theta\right] \tag{41}$$

Note, by comparing Equation (31), that this is of the form

$$G_{2U}(c) = \exp(-\iota\theta)\, G_{LW}(\Delta c) \tag{42}$$

where $\Delta c = c - 1$. Of course, $|\exp(-\iota\theta)| \equiv 1$, and for the "Lax-Wendroff" component based on Δc,

$$|G_{LW}(\Delta c)| \le 1 \quad \text{for} \quad -1 \le \Delta c \le 1 \tag{43}$$

thus proving (40). It should be stressed that second-order upwinding is one well-known explicit advection scheme for which *the CFL condition does not apply*.

In order to gain some insight into the operation of second-order upwinding for a Courant number range of $1 < c \le 2$, Figure 10 shows the situation for $c = 1.25$. In this case, it is not hard to show, using Equation (15), that

$$\begin{aligned} c\phi_t &= \frac{1}{\Delta x}\int_{x_t - c\Delta x}^{x_t - \Delta x} \phi^n(\xi)\,d\xi + \frac{1}{\Delta x}\int_{x_t - \Delta x}^{x_t} \phi^n(\xi)\,d\xi \\ &= \Delta c\left[\frac{1}{2}(\bar{\phi}^n_{i-1} + \bar{\phi}^n_{i-2}) - \frac{\Delta c}{2}(\bar{\phi}^n_{i-1} - \bar{\phi}^n_{i-2})\right] + \bar{\phi}^n_{i-1} \end{aligned} \tag{44}$$

with a similar formula for $c\phi_r$ (with all indexes increased by 1). The term in square brackets is clearly the Lax-Wendroff face-value based on Δc — but for cell $(i-1)$ rather than cell i. This means that the update equation takes the form

$$\bar{\phi}_i^{n+1} = \bar{\phi}_{i-1}^n - \frac{\Delta c}{2}(\bar{\phi}_i^n - \phi_{i-2}^n) + \frac{\Delta c^2}{2}(\bar{\phi}_i^n - 2\bar{\phi}_{i-1}^n + \bar{\phi}_{i-2}^n) \tag{45}$$

with $\Delta c = c - 1$. This is algebraically identical to Equation (35). But, by comparison with Equation (28), it can be seen that the right-hand side is the Lax-Wendroff update of cell $(i-1)$ using Δc rather than c itself. This gives a hint as to how flux-based conservative finite-volume explicit advection schemes might be extended to arbitrarily large Δt. The details will be examined in the next section.

As is well known, the conventional Lax-Wendroff scheme suffers from severe phase-lag dispersion [Fletcher, 1990]. On the other hand, second-order upwinding introduces phase-lead dispersion for $0 < c < 1$. Fromm's method [1968] of "zero-average-phase-error" attempts to minimize the dispersion by taking the arithmetic-mean of the respective sub-grid reconstructions, giving, from Equations (26) and (33)

$$\phi^n(\xi) = \bar{\phi}_{i-1}^n + \left(\frac{\bar{\phi}_i^n - \bar{\phi}_{i-2}^n}{2\Delta x}\right)(\xi - x_{i-1}) \quad \text{for} \quad \left(x_{i-1} - \frac{\Delta x}{2}\right) < \xi < \left(x_{i-1} + \frac{\Delta x}{2}\right) \tag{46}$$

i.e., the slope across any cell is parallel to the chord joining $\bar{\phi}$-values through the centers of the two adjoining cells on either side. This is shown in Figure 11. To compute the face-value, first rewrite Equation (34) for second-order upwinding as

$$\phi_\ell(2U) = \frac{1}{2}(\bar{\phi}_i^n + \bar{\phi}_{i-1}^n) - \frac{c}{2}(\bar{\phi}_i^n - \bar{\phi}_{i-1}^n) - \left(\frac{1-c}{2}\right)(\bar{\phi}_i^n - 2\bar{\phi}_{i-1}^n + \bar{\phi}_{i-2}^n) \tag{47}$$

which is seen to be the Lax-Wendroff value together with a correction term proportional to the upwind-biased second-difference. Then the left face-value for Fromm's method is seen to be, *for Courant number less than (or equal to) one*,

$$\begin{aligned}\phi_\ell(\text{Fromm}) &= \frac{1}{2}[\phi_\ell(\text{LW}) + \phi_\ell(2U)] \\ &= \frac{1}{2}(\bar{\phi}_i^n + \bar{\phi}_{i-1}^n) - \frac{c}{2}(\bar{\phi}_i^n - \bar{\phi}_{i-1}^n) - \left(\frac{1-c}{4}\right)(\bar{\phi}_i^n - 2\bar{\phi}_{i-1}^n + \bar{\phi}_{i-2}^n)\end{aligned} \tag{48}$$

and the corresponding update equation becomes

$$\begin{aligned}\bar{\phi}_i^{n+1} = \bar{\phi}_i^n &- \frac{c}{2}(\bar{\phi}_{i+1}^n - \bar{\phi}_{i-1}^n) + \frac{c^2}{2}(\bar{\phi}_{i+1}^n - 2\bar{\phi}_i^n + \bar{\phi}_{i-1}^n) \\ &+ c\left(\frac{1-c}{4}\right)(\bar{\phi}_{i+1}^n - 3\bar{\phi}_i^n + 3\bar{\phi}_{i-1}^n - \bar{\phi}_{i-2}^n)\end{aligned} \tag{49}$$

with a complex amplitude ratio

$$\mathbf{G}_{\text{Fr}}(c) = \mathbf{G}_{\text{LW}}(c) + c\left(\frac{1-c}{4}\right)[\exp(\imath\theta) - 3 + 3\exp(-\imath\theta) - \exp(-\imath 2\theta)] \tag{50}$$

or

$$G_{Fr}(c) = 1 - c^2(1-\cos\theta) - c\left(\frac{1-c}{2}\right)(1-\cos\theta)^2 - \iota\left[c\sin\theta + c\left(\frac{1-c}{2}\right)\sin\theta\,(1-\cos\theta)\right] \tag{51}$$

This has a Taylor expansion

$$G_{Fr}(c) = 1 - \frac{c^2}{2}\theta^2 + O(\theta^4) - \iota\left[c\theta - \left(\frac{3c^2-c}{12}\right)\theta^3 + O(\theta^5)\right] \tag{52}$$

Although this is only formally second-order accurate, the θ^3 coefficient is a fairly good approximation of the exact coefficient, $c^3/6$, over the operating range, $0 < c \leq 1$. From its formulation as the average of Lax-Wendroff and second-order upwinding, Fromm's method clearly *needs to satisfy the CFL condition* for stability.

Higher-Order Methods

In order to construct a higher-order approximation for estimating a face-value, say ϕ_ℓ, one might try to interpolate a parabola across cell $(i-1)$ passing through the three values, $\bar{\phi}^n_{i-2}$, $\bar{\phi}^n_{i-1}$, and $\bar{\phi}^n_i$ (for $u > 0$), with the location of these values considered to be at the center of their respective cells. Such a parabola is shown by a dashed line in Figure 12. But, of course, this does not generally satisfy the integral condition given by Equation (17). Because of its curvature, the parabola needs to be shifted vertically to satisfy this constraint. Thus, by introducing an additional constant, $\phi^n(\xi)$ can be written, in the upstream vicinity of the left face, as

$$\phi^n(\xi) = C_1 + \bar{\phi}^n_{i-1} + \left(\frac{\bar{\phi}^n_i - \bar{\phi}^n_{i-2}}{2\Delta x}\right)(\xi - x_{i-1}) + \left(\frac{\bar{\phi}^n_i - 2\bar{\phi}^n_{i-1} + \bar{\phi}^n_{i-2}}{2\Delta x^2}\right)(\xi - x_{i-1})^2 \tag{53}$$

for $\left(x_{i-1} - \frac{\Delta x}{2}\right) \leq \xi \leq \left(x_{i-1} + \frac{\Delta x}{2}\right)$. Substitution into Equation (17), rewritten for cell $(i-1)$, then gives

$$C_1 = -\left(\frac{\bar{\phi}^n_i - 2\bar{\phi}^n_{i-1} + \bar{\phi}^n_{i-2}}{24}\right) \tag{54}$$

The corresponding parabolic segment across cell $(i-1)$ is shown by a heavy curve in Figure 12. Then Equation (15) gives the corresponding left-face value, for Courant number *less than (or equal to) one*, as

$$\phi_\ell = \frac{1}{2}\left(\bar{\phi}^n_i + \bar{\phi}^n_{i-1}\right) - \frac{c}{2}\left(\bar{\phi}^n_i - \bar{\phi}^n_{i-1}\right) - \left(\frac{1-c^2}{6}\right)\left(\bar{\phi}^n_i - 2\bar{\phi}^n_{i-1} + \bar{\phi}^n_{i-2}\right) \tag{55}$$

with a similar formula for ϕ_r ($i \to i+1$, as usual). The corresponding update equation is

$$\bar{\phi}_i^{n+1} = \bar{\phi}_i^n - \frac{c}{2}\left(\bar{\phi}_{i+1}^n - \bar{\phi}_{i-1}^n\right) + \frac{c^2}{2}\left(\bar{\phi}_{i+1}^n - 2\bar{\phi}_i^n + \bar{\phi}_{i-1}^n\right) + c\left(\frac{1-c^2}{6}\right)\left(\bar{\phi}_{i+1}^n - 3\bar{\phi}_i^n + 3\bar{\phi}_{i-1}^n - \bar{\phi}_{i-2}^n\right) \tag{56}$$

This has the same form as the third-order upwind QUICKEST scheme [Leonard 1979], but in terms of *cell-average* values, $\bar{\phi}$, rather than *nodal* values. But note from Equations (53) and (54) that a nodal value can be retrieved from the sub-grid behaviour. For cell $(i-1)$, for example, the nodal value is

$$\phi_{i-1} = \phi^n(x_{i-1}) = \bar{\phi}_{i-1}^n - \left(\frac{\bar{\phi}_i^n - 2\bar{\phi}_{i-1}^n + \bar{\phi}_{i-2}^n}{24}\right) \tag{57}$$

This means that the QUICKEST scheme can be constructed from Equation (56) by writing

$$\phi_i^{n+1} = \bar{\phi}_i^{n+1} - \left(\frac{\bar{\phi}_{i+1}^{n+1} - 2\bar{\phi}_i^{n+1} + \bar{\phi}_{i-1}^{n+1}}{24}\right) \quad \text{for all } i \tag{58}$$

giving

$$\phi_i^{n+1} = \phi_i^n - \frac{c}{2}\left(\phi_{i+1}^n - \phi_i^n\right) + \frac{c^2}{2}\left(\phi_{i+1}^n - 2\phi_i^n + \phi_{i-1}^n\right) + c\left(\frac{1-c^2}{6}\right)\left(\phi_{i+1}^n - 3\phi_i^n + 3\phi_{i-1}^n - \phi_{i-2}^n\right) \tag{59}$$

for $0 < c \leq 1$, thus matching the original QUICKEST algorithm, for pure convection.

From the similarity with Fromm's method, the complex amplitude ratio can be immediately written down as

$$\mathbf{G}_Q(c) = 1 - c^2\,(1-\cos\theta) - c\left(\frac{1-c^2}{3}\right)(1-\cos\theta)^2 - \imath\left[c\,\sin\theta + c\left(\frac{1-c^2}{3}\right)\sin\theta\,(1-\cos\theta)\right] \tag{60}$$

and, in this case, the Taylor expansion matches $\mathbf{G}_{\text{exact}}$, Equation (25), through third-order terms

$$\mathbf{G}_Q(c) = 1 - \frac{c^2}{2}\,\theta^2 + O(\theta^4) - \imath\left[c\theta - \frac{c^3}{6}\,\theta^3 + O(\theta^5)\right] \tag{61}$$

verifying the expected third-order accuracy.

Higher-order methods can be constructed in a similar fashion. If a Pth-order piecewise polynomial (or spline, for that matter) is used for the sub-grid reconstruction, satisfying Equation (17), the resulting advection scheme will be $(P+1)$th-order accurate. This pattern has already been seen for first- through third-order methods.

LARGE TIME-STEP EXTENSION

Most conventional explicit advection schemes are constructed on the *assumption* that the Courant number will be in the range $0 < c \leq 1$ in computing time-averaged face-values; note the conditional statements just before Equations (19), (26), (48), and (55). It is not surprising, then, that such methods need to satisfy the CFL condition ($|c| \leq 1$) for stability — the notable exception being second-order upwinding, which, somewhat fortuitously, is stable for $0 < c \leq 2$. Referring again to Figure 10, it can be seen that second-order upwinding, for $c > 1$, is equivalent to a "Lax-Wendroff type" of sub-grid reconstruction over each cell (compare cell i-2 in Figures 4 and 10); i.e., for each cell i,

$$\phi^n(\xi) = \bar{\phi}_i^n + \left(\frac{\bar{\phi}_{i+1}^n - \bar{\phi}_i^n}{\Delta x}\right)(\xi - x_i) \tag{62}$$

for $u > 0$. Then, since the integration in Equation (15) is over more than one cell, the average left face, for example, can be written

$$c\phi_l(i) = \bar{\phi}_{i-1}^n + \Delta c\, \phi_l^{LW}(i-1, \Delta c) \tag{63}$$

where the notation implies that $\phi_l^{LW}(i-1, \Delta c)$ is the left-face value of cell $(i-1)$ that would have been obtained for a Lax-Wendroff scheme with a Courant number of Δc ($= c - 1$, in this case).

Clearly, this idea could be extended to even larger Courant number. For example, Figure 13 shows a situation for $c = 2.625$. In this case, it should be clear that

$$c\phi_l(i) = \bar{\phi}_{i-1}^n + \bar{\phi}_{i-2}^n + \Delta c\, \phi_l^{LW}(i-2, \Delta c) \tag{64}$$

where $\Delta c = c - 2$. Of course, the right-face value is given by Equation (16), or

$$c\phi_r(i) = \bar{\phi}_i^n + \bar{\phi}_{i-1}^n + \Delta c\, \phi_l^{LW}(i-1, \Delta c) \tag{65}$$

The update equation then becomes

$$\bar{\phi}_i^{n+1} = \bar{\phi}_i^n - \left[\bar{\phi}_i^n + \bar{\phi}_{i-1}^n + \Delta c\, \phi_l^{LW}(i-1, \Delta c)\right] + \left[\bar{\phi}_{i-1}^n + \bar{\phi}_{i-2}^n + \Delta c\, \phi_l^{LW}(i-2, \Delta c)\right] \tag{66}$$

resulting in an effective update of the form

$$\bar{\phi}_i^{n+1} = \bar{\phi}_{i-2}^n - \Delta c\left[\phi_l^{LW}(i-1, \Delta c) - \phi_l^{LW}(i-2, \Delta c)\right] \tag{67}$$

or, more specifically, using the sub-grid (i.e., "Lax-Wendroff-type") reconstruction of Equation (62),

$$\bar{\phi}_i^{n+1} = \bar{\phi}_{i-2}^n - \frac{\Delta c}{2}\left(\bar{\phi}_{i-1}^n - \bar{\phi}_{i-3}^n\right) + \frac{\Delta c^2}{2}\left(\bar{\phi}_{i-1}^n - 2\bar{\phi}_{i-2}^n + \bar{\phi}_{i-3}^n\right) \tag{68}$$

It is not hard to see that this idea generalizes to (in principle) arbitrarily large Courant number, in which case

$$c\phi_t(i) = \sum_{p=1}^{N} \bar{\phi}^n_{i-p} + \Delta c\, \phi_t^{LW}(i-N, \Delta c) \tag{69}$$

with a corresponding formula for $c\phi_r(i)$, according to Equation (16). The effective ("extended Lax-Wendroff") update equation is then

$$\bar{\phi}^{n+1}_i = \bar{\phi}^n_{i-N} - \frac{\Delta c}{2}\left(\bar{\phi}^n_{i-N+1} - \bar{\phi}^n_{i-N-1}\right) + \frac{\Delta c^2}{2}\left(\bar{\phi}^n_{i-N+1} - 2\bar{\phi}^n_{i-N} + \bar{\phi}^n_{i-N-1}\right) \tag{70}$$

Of course, the same principle could be applied to *any* sub-grid reconstruction. Then, one simply writes for the left face, say,

$$c\phi_t(i) = \sum_{p=1}^{N} \bar{\phi}^n_{i-p} + \Delta c\, \phi_t(i-N, \Delta c) \tag{71}$$

where $\phi_t(i-N, \Delta c)$ is computed at the left-face of cell $(i-N)$ based on a Courant number of Δc. The update equation is then

$$\bar{\phi}^{n+1}_i = \bar{\phi}^n_i - [c\phi_t(i+1) - c\phi_t(i)] \tag{72}$$

as usual. And this is equivalent to

$$\bar{\phi}^{n+1}_i = \bar{\phi}_{i-N} - \Delta c\, [\phi_t(i-N+1, \Delta c) - \phi_t(i-N, \Delta c)] \tag{73}$$

Stability Analysis

Consider a von Neumann stability analysis of the extended Lax-Wendroff update equation, Equation (70). The complex amplitude ratio is

$$\begin{aligned} G_{ELW} = \exp(-\imath N\theta) &- \frac{\Delta c}{2}\left\{\exp[-\imath(N-1)\theta] - \exp[-\imath(N+1)\theta]\right\} \\ &+ \frac{\Delta c^2}{2}\left\{\exp[-\imath(N-1)\theta] - 2\exp(-\imath N\theta) + \exp[-\imath(N+1)\theta]\right\} \end{aligned} \tag{74}$$

which can be rewritten as

$$\begin{aligned} G_{ELW} = \exp(-\imath N\theta) \Big\{1 &- \frac{\Delta c}{2}\left[\exp(\imath\theta) - \exp(-\imath\theta)\right] \\ &+ \frac{\Delta c^2}{2}\left[\exp(\imath\theta) - 2 + \exp(-\imath\theta)\right]\Big\} \end{aligned} \tag{75}$$

or, by comparison with Equation (30),

$$G_{ELW} = \exp(-\imath N\theta)\, G_{LW}(\Delta c) \tag{76}$$

where $\Delta c = c - N$. Since $\Delta c < 1$, by definition, the extended Lax-Wendroff scheme is clearly stable.

The formula can be generalized to any scheme (i.e., any sub-grid reconstruction) for which the face-value is a linear combination of cell-average values. For such schemes, the large time-step (LTS) G can always be factored into the form

$$\mathbf{G}_{\mathrm{LTS}} = \exp(-\imath N\theta)\ \mathbf{G}_{\mathrm{STS}}(\Delta c) \tag{77}$$

And if $|\mathbf{G}_{\mathrm{STS}}(\Delta c)| < 1$, for $\Delta c < 1$, the LTS scheme is stable. The formal order of accuracy of $\mathbf{G}_{\mathrm{LTS}}$ is the same as that of $\mathbf{G}_{\mathrm{STS}}(\Delta c)$.

LARGE TIME-STEP EXPLICIT TVD SCHEMES

Total-variation-diminishing (TVD) schemes, as described by Sweby [1984], for example, involve face-values that are, in general, nonlinear functions of (local) cell-average values. The TVD constraint boundaries described by Sweby have a simple interpretation in terms of sub-grid reconstruction. The explicit large-time-step extension is then quite straightforward, although the von Neumann stability analysis is somewhat more involved (even for the case of $c < 1$).

First, for definiteness, consider the case of $c < 1$. The left-face value is based on a linear reconstruction across cell $(i-1)$ satisfying Equation (17), but with a slope determined by certain "limiter" constraints. It is convenient to define

$$\phi_t^0 = \phi_t(c \to 0) \tag{78}$$

This is shown in Figure 14. The TVD value of ϕ_t^0 is usually written as

$$\phi_t^0(\mathrm{TVD}) = \bar{\phi}_{i-1}^n - \varphi\left[\bar{\phi}_{i-1}^n - \frac{1}{2}\left(\bar{\phi}_i^n + \bar{\phi}_{i-1}^n\right)\right] \tag{79}$$

interpreted as first-order upwinding, corrected by a term proportional to the difference between first-order upwinding and second-order central (i.e., linear) interpolation between $\bar{\phi}_{i-1}^n$ and $\bar{\phi}_i^n$, as shown in the figure. The factor φ is the antidiffusion flux-limiter factor, and is a nonlinear function of the local gradient ratio

$$r = \frac{\left(\bar{\phi}_{i-1}^n - \bar{\phi}_{i-2}^n\right)}{\left(\bar{\phi}_i^n - \bar{\phi}_{i-1}^n\right)} \tag{80}$$

Equation (79) can be rewritten as

$$\phi_t^0(\mathrm{TVD}) = \frac{1}{2}\left(\bar{\phi}_i^n + \bar{\phi}_{i-1}^n\right) - \frac{(1-\varphi)}{2}\left(\bar{\phi}_i^n - \bar{\phi}_{i-1}^n\right) \tag{81}$$

The time-averaged face-value (for $c \leq 1$) is then, from Equation (15),

$$\phi_t(\text{TVD}) = (1-c)\phi_t^0 + c\,\bar{\phi}_{i-1}^n \tag{82}$$

giving

$$\phi_t(\text{TVD}) = \phi_t^{\text{LW}} - \frac{1}{2}(1-\varphi)(1-c)\left(\bar{\phi}_i^n - \bar{\phi}_{i-1}^n\right) \tag{83}$$

where the coefficient of the latter term can be viewed as being proportional to an effective artificial diffusivity (or viscosity)

$$D_{\text{art}} = \frac{1}{2}(1-\varphi)(1-c)\,u\,\Delta x \tag{84}$$

relative to the Lax-Wendroff face-value.

Sweby gives the TVD constraints on φ as

$$\varphi = 0 \quad \text{for} \quad r \le 0 \tag{85}$$

$$0 \le \varphi \le 2r \quad \text{for} \quad 0 < r \le 1 \tag{86}$$

and

$$0 \le \varphi \le 2 \quad \text{for} \quad r > 2 \tag{87}$$

This is shown in Figure 15. Figure 16 shows three typical examples for $r = -1/2, +1/3,$ and 3. For a local maximum (or minimum), case (a),

$$\phi_t = \phi_t^0 = \bar{\phi}_{i-1}^n, \quad r \le 0 \tag{88}$$

In the other cases, the sub-grid reconstruction across cell $(i-1)$ is a linear function passing through $\bar{\phi}_{i-1}^n$ at x_i

$$\phi^n(\xi) = \bar{\phi}_{i-1}^n + S(\xi - x_{i-1}) \tag{89}$$

where the slope, S, is constrained to satisfy

$$0 \le |S| \le |S_{\text{con}}| \tag{90}$$

For a gradient increasing (in magnitude) with i (i.e., $0 < r \le 1$), case (b), the constrained slope is

$$S_{\text{con}} = \frac{\left(\bar{\phi}_{i-1}^n - \bar{\phi}_{i-2}^n\right)}{\Delta x/2} \tag{91}$$

corresponding to $\varphi = 2r$, or $\phi_t^0 = 2\bar{\phi}_{i-1}^n - \bar{\phi}_{i-2}^n$. And for $r > 1$, case (c),

$$S_{\text{con}} = \frac{\left(\bar{\phi}_i^n - \bar{\phi}_{i-1}^n\right)}{\Delta x/2} \tag{92}$$

corresponding to $\varphi = 2$, or $\phi_t^0 = \bar{\phi}_i^n$. The limiting slope, S_{con}, is thus seen to be the *smaller* (in magnitude) of *twice* the backward or forward gradient; the *larger* value is shown by the chain-dashed line in each case in Figure 16.

Although explicit TVD schemes have been used only for time-steps satisfying the CFL condition, *there is clearly no need for this constraint*. Figure 17 shows a reconstruction that uses S_{con} across each cell, with a Courant number of $c = 2.25$. In this case,

$$c\,\phi_t(i) = \bar{\phi}_{i-1}^n + \bar{\phi}_{i-2}^n + \Delta c\,\phi_t(i-2) \tag{93}$$

where

$$\Delta c\,\phi_t(i-2) = \Delta c\left[\bar{\phi}_{i-3}^n + (1-\Delta c)\,S_{con}\,\Delta x/2\right] \tag{94}$$

or, in this case (since $r > 1$),

$$\Delta c\,\phi_t(i-2) = \Delta c\,\bar{\phi}_{i-3}^n + \Delta c\,(1-\Delta c)\left(\bar{\phi}_{i-2}^n - \bar{\phi}_{i-3}^n\right) \tag{95}$$

And the right-face value is given by

$$c\,\phi_r(i) = c\,\phi_t(i+1) = \bar{\phi}_i^n + \bar{\phi}_{i-1}^n + \Delta c\,\phi_t(i-1) \tag{96}$$

or (since, here, $r < 1$)

$$c\,\phi_r(i) = \bar{\phi}_i^n + \bar{\phi}_{i-1}^n + \Delta c\,\bar{\phi}_{i-2}^n + \Delta c\,(1-\Delta c)\left(\bar{\phi}_{i-2}^n - \bar{\phi}_{i-3}^n\right) \tag{97}$$

for the case shown. The update equation is then, effectively,

$$\bar{\phi}_i^{n+1} = \bar{\phi}_{i-2}^n - \Delta c\left(\bar{\phi}_{i-2}^n - \bar{\phi}_{i-3}^n\right) \tag{98}$$

in this case, equivalent to (extended) first-order upwinding. The complex amplitude ratio (for cell i) is

$$\mathbf{G}_i = \exp(-\imath 2\theta)\,\{1 - 0.25[1 - \exp(-\imath\theta)]\} \tag{99}$$

which is stable, the term in square brackets being $\mathbf{G}_{1U}(\Delta c)$.

In general, for $c = N + \Delta c$, the complex amplitude ratio will vary from cell to cell, depending on the particular form of sub-grid reconstruction near cell $(i - N)$, but, in any case,

$$\mathbf{G}_i = \exp(-\imath N\theta)\;\mathbf{G}_{i-N}(\Delta c) \tag{100}$$

using an obvious notation. Since, for TVD schemes, $|\mathbf{G}_{i-N}(\Delta c)| < 1$ for $\Delta c < 1$, the large time-step extension is always stable.

CONCLUSION

Most conventional explicit advection schemes need to satisfy the CFL condition ($c \leq 1$) because of a *restriction on the range of validity of the sub-grid reconstruction formula* upstream of individual finite-volume faces. If the given formula for the sub-grid reconstruction (valid for $c \leq 1$) is extended beyond $c = 1$, the scheme is unstable in the von Neumann sense (except for second-order upwinding, which is stable for $0 < c \leq 2$). For example, Figure 18 shows an extension of the conventional Lax-Wendroff sub-grid reconstruction upstream of the left face of cell i, for $c = 1.75$,

$$\phi^n(\xi) \;=\; \bar{\phi}^n_{i-1} + \left(\frac{\bar{\phi}^n_i - \bar{\phi}^n_{i-1}}{\Delta x}\right)(\xi - x_{i-1}) \tag{101}$$

Clearly, the real problem is that, across cell $(i-2)$, $\phi^n(\xi)$ *does not satisfy the consistency relationship* of Equation (17); i.e.,

$$\int_{x_{i-2}-\Delta x/2}^{x_{i-2}+\Delta x/2} \phi^n(\xi)\,d\xi \;\neq\; \bar{\phi}^n_{i-2} \tag{102}$$

In the case shown, the influx through the left face of cell i will be too small (and the outflux through the right, far too large) resulting in a wild oscillation of $\bar{\phi}_i$ that rapidly grows without limit.

Second-order upwind sub-grid reconstruction upstream of the left face of cell i, (somewhat fortuitously) satisfies Equation (17) for *both* cell $(i-1)$ *and* $(i-2)$. This is the fundamental reason for the stability range extending to $c = 2$. Once this is recognized, it is not hard to see how to generalize to arbitrarily large Courant number. One simply performs a sub-grid reconstruction satisfying Equation (17), then computes all face-values according to Equation (15), or, equivalently,

$$c\,\phi_t(i) \;=\; \sum_{p=1}^{N} \bar{\phi}^n_{i-p} + \Delta c\,\phi_t(i-N, \Delta c) \tag{103}$$

finally updating *via*

$$\bar{\phi}^{n+1}_i \;=\; \bar{\phi}^n_i - c\left[\phi_t(i+1) - \phi_t(i)\right] \tag{104}$$

The result is equivalent to

$$\bar{\phi}^{n+1}_i \;=\; \bar{\phi}^n_{i-N} - \Delta c\left[\phi_t(i-N+1, \Delta c) - \phi_t(i-N, \Delta c)\right] \tag{105}$$

representing an update of cell-average $\bar{\phi}_{i-N}$ for a Courant number of Δc, together with a simple *translation* over N mesh-widths. It should be clear that any numerical distortion of the evolved profile depends on the particular form of sub-grid reconstruction, the total number of time-steps, and Δc—but not on c itself.

A piece-wise constant assumption across each cell results in a *very diffusive* first-order scheme. A Lax-Wendroff-type sub-grid reconstruction, as given by Equation (26) for each cell, gives rise to *trailing oscillations*, just as in the conventional ($c < 1$) case. Conversely,

the large time-step (LTS) extension of second-order upwinding, given by Equation (33) for each cell, results in *leading oscillations*. The extended version of Fromm's method, Equation (46), and particularly QUICKEST, Equation (53), are much less oscillatory. Finally, for large-Δt explicit TVD schemes, the evolved shape is nonoscillatory, identical to that for a Courant number of Δc (< 1) for the same number of time-steps, but translated N mesh-widths downstream.

Note that some sub-grid interpolations are independent of the direction of the convecting velocity. This is the case, for example, with (the large-Δt extension of) first-order upwinding, Fromm's method, and QUICKEST's piecewise-parabolic interpolation; the reconstruction is the same, no matter whether c is positive or negative. In these cases, there is a sort of built-in ''natural upwind bias'' because of the way the fluxes are calculated. A second-order upwind type reconstruction based on (for $c > 0$)

$$\phi^n(\xi) \;=\; \bar{\phi}_i^n + \left(\frac{\bar{\phi}_i^n - \bar{\phi}_{i-1}^n}{\Delta x}\right)(\xi - x_i) \tag{106}$$

across each cell i, has an additional upwind bias. For $c < 0$, the corresponding formula would be

$$\phi^n(\xi) \;=\; \bar{\phi}_i^n + \left(\frac{\bar{\phi}_{i+1}^n - \bar{\phi}_i^n}{\Delta x}\right)(\xi - x_i) \tag{107}$$

By contrast, the Lax-Wendroff type reconstruction uses Equation (107) for $c > 0$ and Equation (106) for $c < 0$; this is a form of *downwind* bias. Generally, the direction-insensitive schemes have better phase accuracy than the ''directional'' schemes.

A von Neumann stability analysis of the large-time-step explicit scheme always results in a complex amplitude ratio of the form

$$\mathbf{G}_{\mathrm{LTS}} \;=\; \exp(-\imath N\theta)\;\mathbf{G}_{\mathrm{STS}}(\Delta c) \tag{108}$$

which should be compared with the exact expression, rewritten here for convenience

$$\mathbf{G}_{\mathrm{exact}} \;=\; \exp(-\imath N\theta)\exp(-\imath \Delta c\,\theta) \tag{109}$$

Generalization of the one-dimensional LTS schemes to variable mesh-widths and (some specific forms of) varying velocity fields appears to be relatively straight-forward. Such schemes have recently been explored by Roache [1992]. Extension to two (and three) dimensions is much more challenging; but some progress has been made. This will be reported in future publications.

REFERENCES

Fletcher, C.A.J., *Computational Techniques for Fluid Dynamics*, Vols. I and II, Springer-Verlag, New York (1990).

Fromm, J.E., 'A Method for Reducing Dispersion in Convective Difference Schemes', *Journal of Computational Physics*, **3**, 176-189 (1968).

Lax, P.D. and B. Wendroff, 'Systems of Conservation Laws', *Communications on Pure and Applied Mathematics*, **13**, 217-237 (1960).

Leith, C.E., 'Numerical Simulation of the Earth's Atmosphere', *Methods in Computational Physics*, **4**, 1-28 (1965).

Leonard, B.P., 'A Stable and Accurate Convective Modelling Procedure Based on Quadratic Upstream Interpolation', *Computer Methods in Applied Mechanics and Engineering*, **19**, 59-98 (1979).

Leonard, B.P., 'Note on the von Neuman Stability of the Explicit FTCS Convective Diffusion Equation', *Applied Mathematical Modelling*, **4**, 401-402 (1980).

Roache, Patrick J., 'A Flux-Based Modified Method of Characteristics', *International Journal for Numerical Methods in Fluids*, **15**, 1259-1275 (1992).

Sweby, P.K., 'High Resolution Schemes Using Flux Limiters for hyperbolic Conservation Laws', *SIAM Journal of Numerical Analysis*, **21**, 995-1011 (1984).

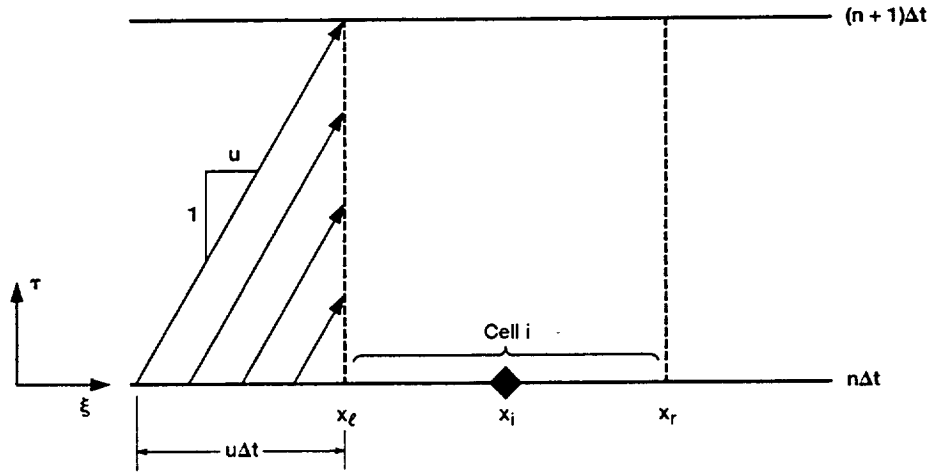

Figure 1.—Space-time grid showing advective characterisitics into the left face of finite-volume cell i.

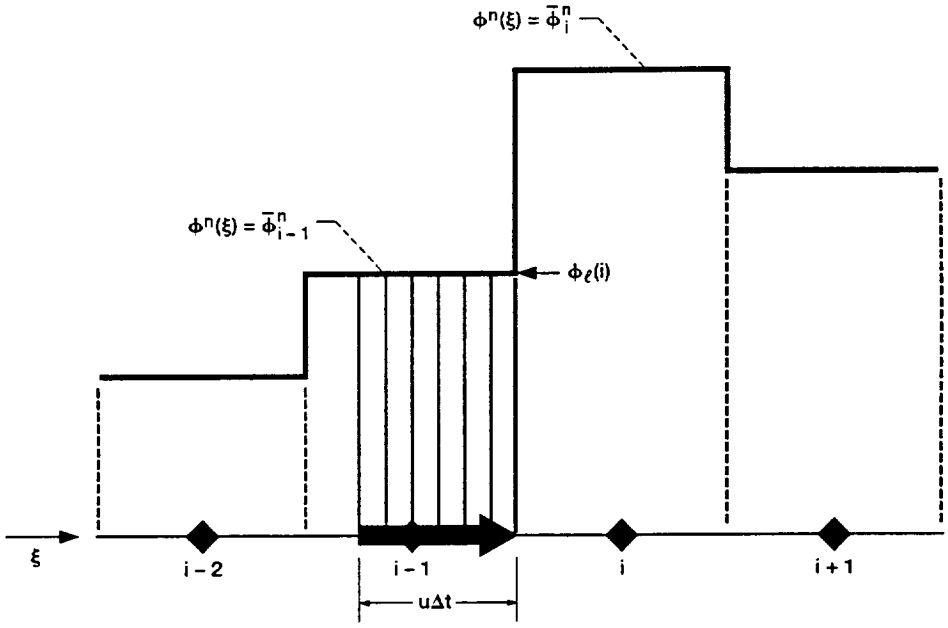

Figure 2.—Piece-wise constant sub-grid behavior. The hatched region represents influx into the left face of cell i, for c = 0.75.

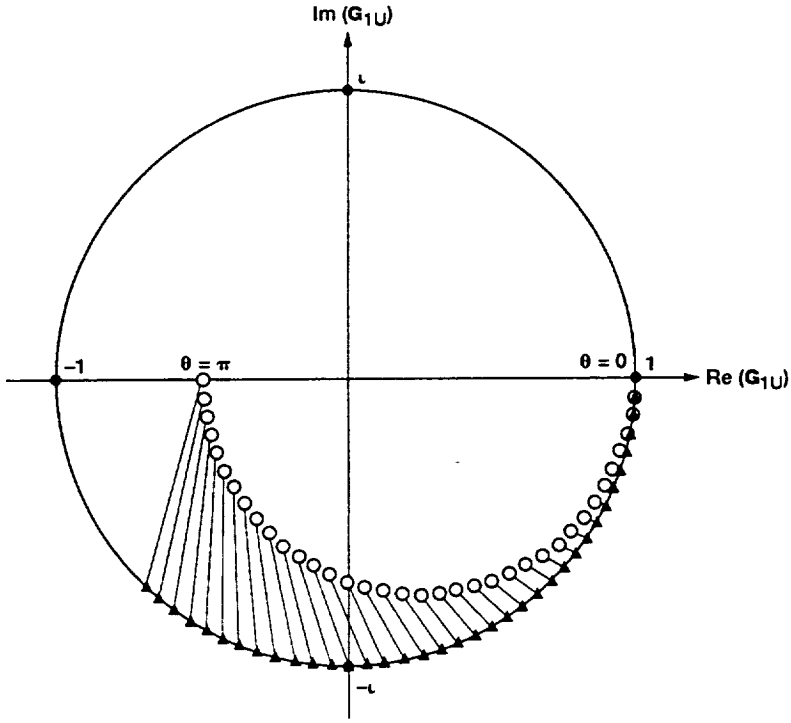

Figure 3.—Polar plot of G_{1U} for c = 0.75. This is a semi-circle in the lower half of the G-plane. Data points are connected to exact G values at corresponding θ values, for 5° increments in θ.

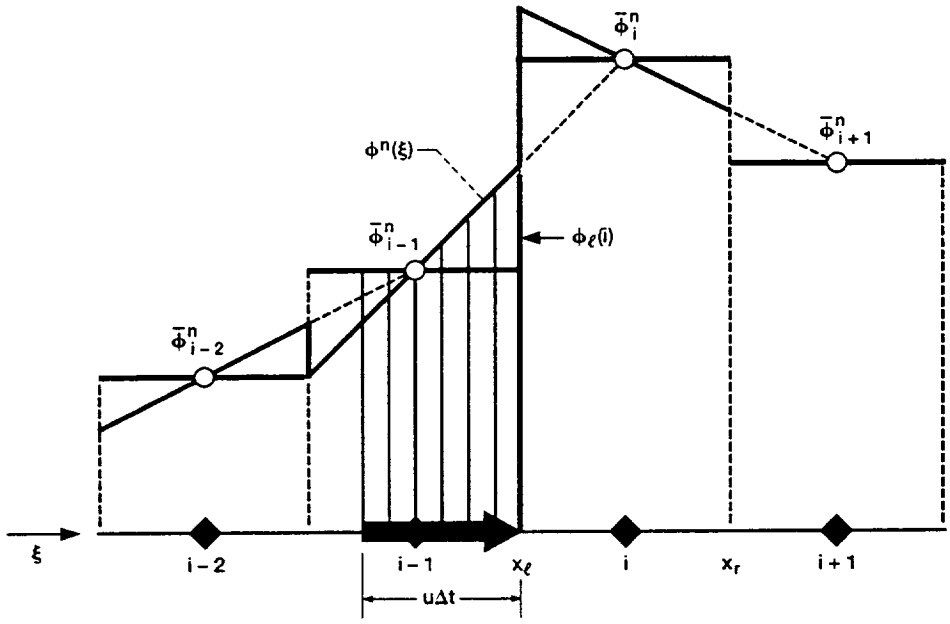

Figure 4.—Conventional Lax-Wendroff sub-grid reconstruction. The hatched region represents left-face influx for cell i, for c = 0.75.

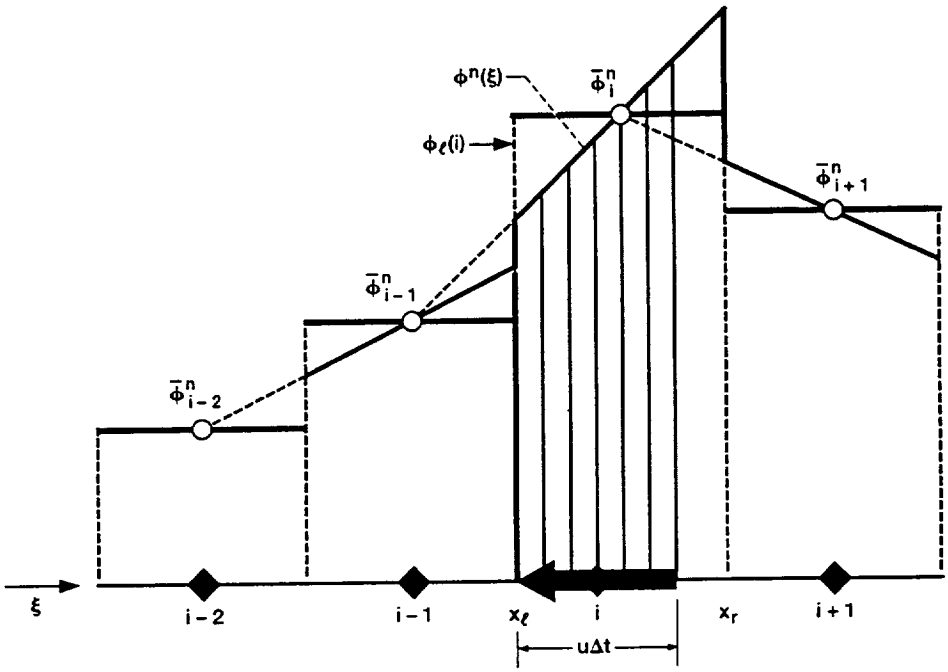

Figure 5.—Conventional Lax-Wendroff sub-grid reconstruction for negative Courant number, c = −0.75.

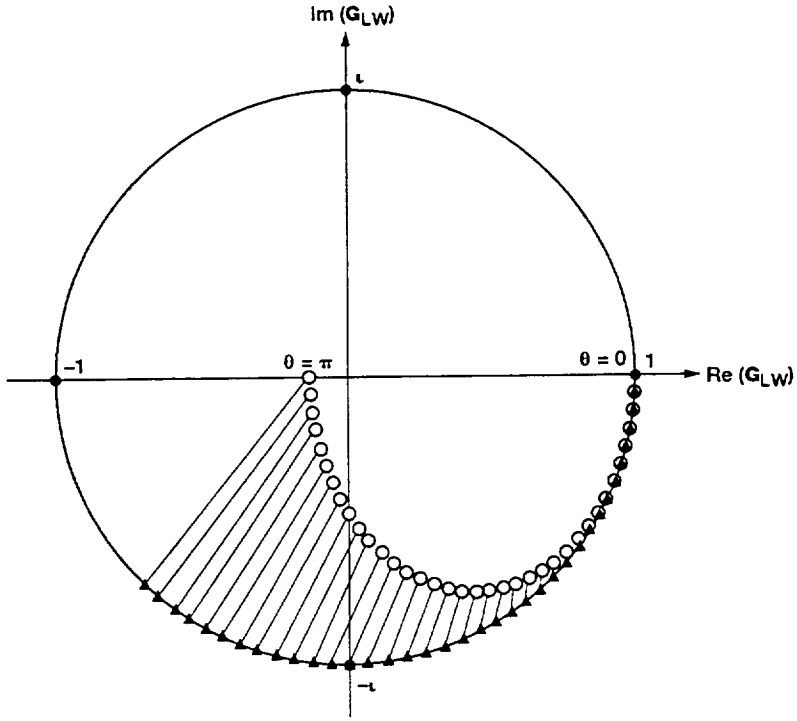

Figure 6.—Polar plot of G_{LW} for c = 0.75. This is a semi-ellipse in the lower half of the G-plane. Exact values also shown, with 5° increments in θ.

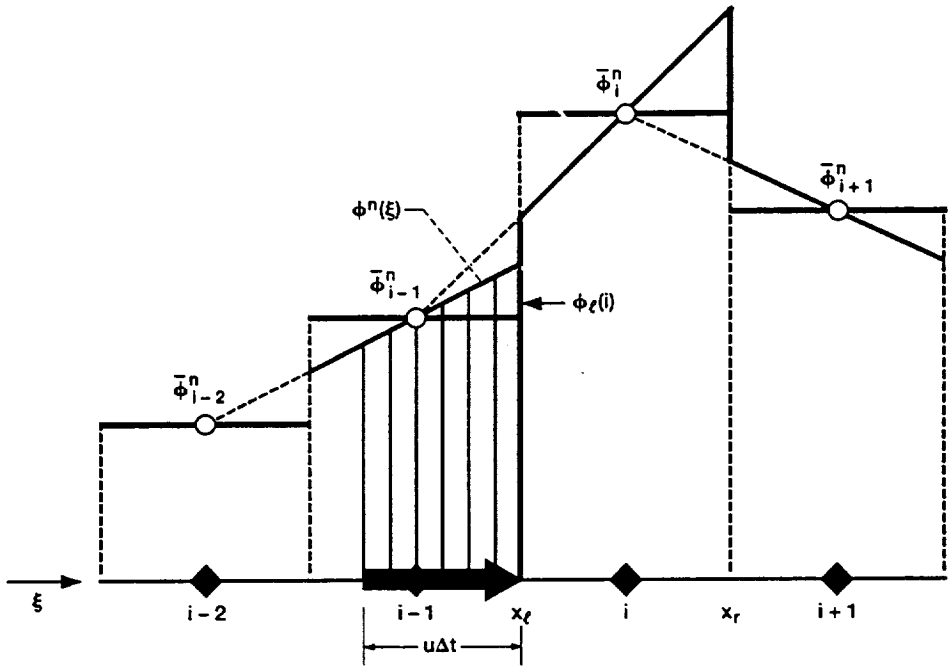

Figure 7.—Conventional second-order sub-grid reconstruction for positive c (= −0.75).

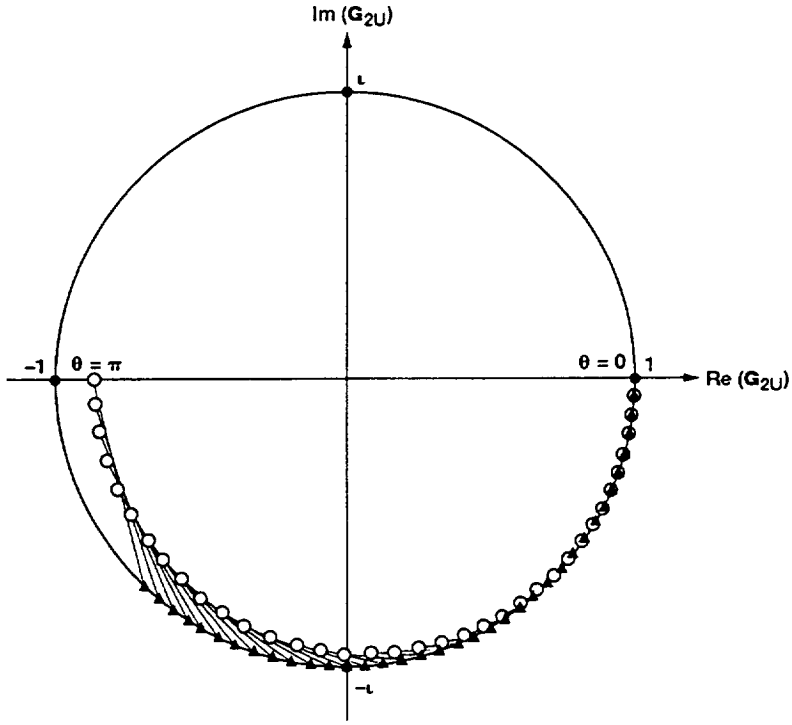

Figure 8.—Polar plot of G_{2U} for c = 0.75. Exact values also shown, with 5° increments in θ.

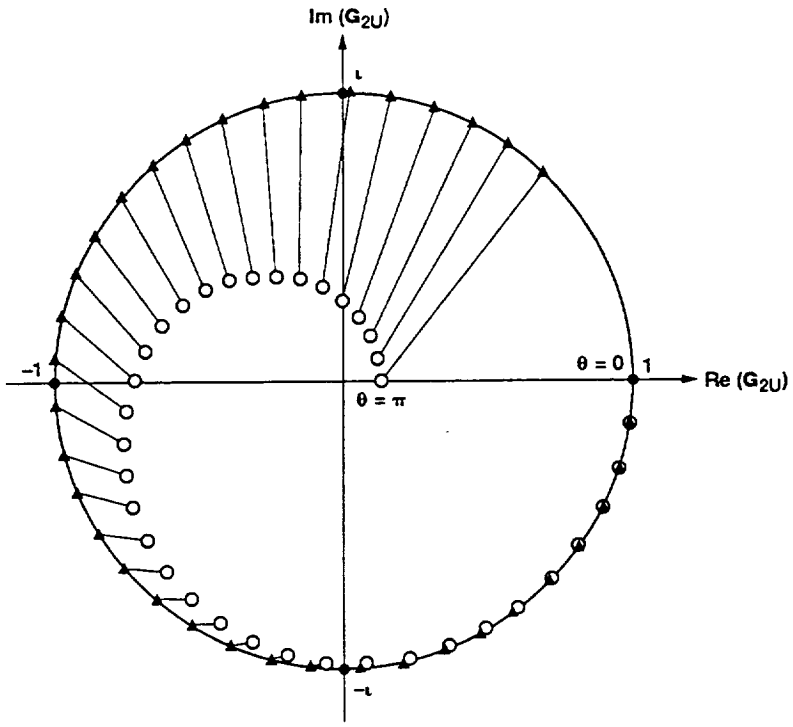

Figure 9.—Polar plot of G_{2U} for c = 1.75. Exact values also shown, with 5° increments in θ.

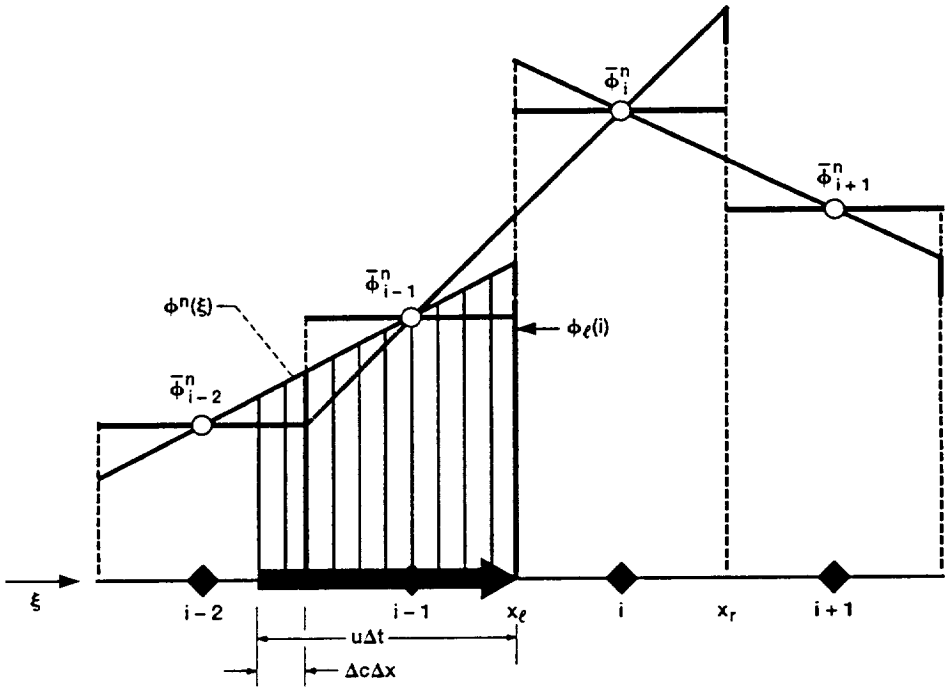

Figure 10.—Conventional second-order upwinding, c = 1.25. Face influxes require integration over more than one cell. Because of the double-valued interpolation, the small vertical ticks indicate which faces belong to which interpolant.

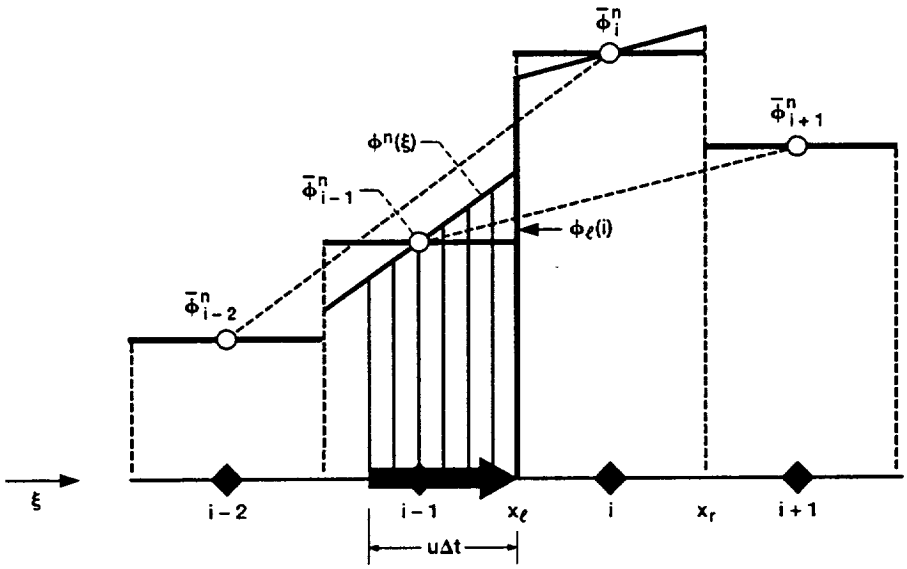

Figure 11.—Sub-grid reconstruction for Fromm's method. The slope of the interpolant across any cell is parallel to the chord joining adjacent cell-averages. In this case, c = 0.75.

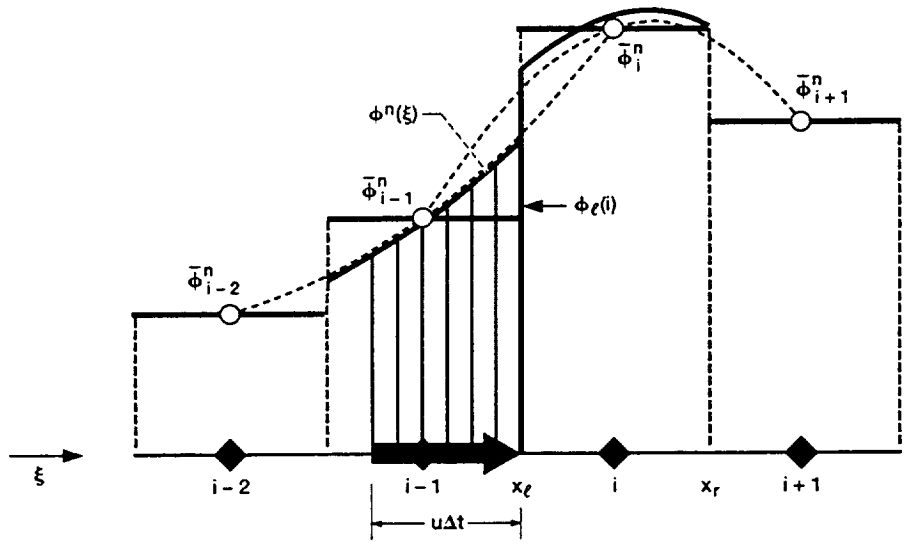

Figure 12.—Piece-wise parabolic interpolation across cells, resulting in a third-order upwind scheme equivalent to QUICKEST; c = 0.75.

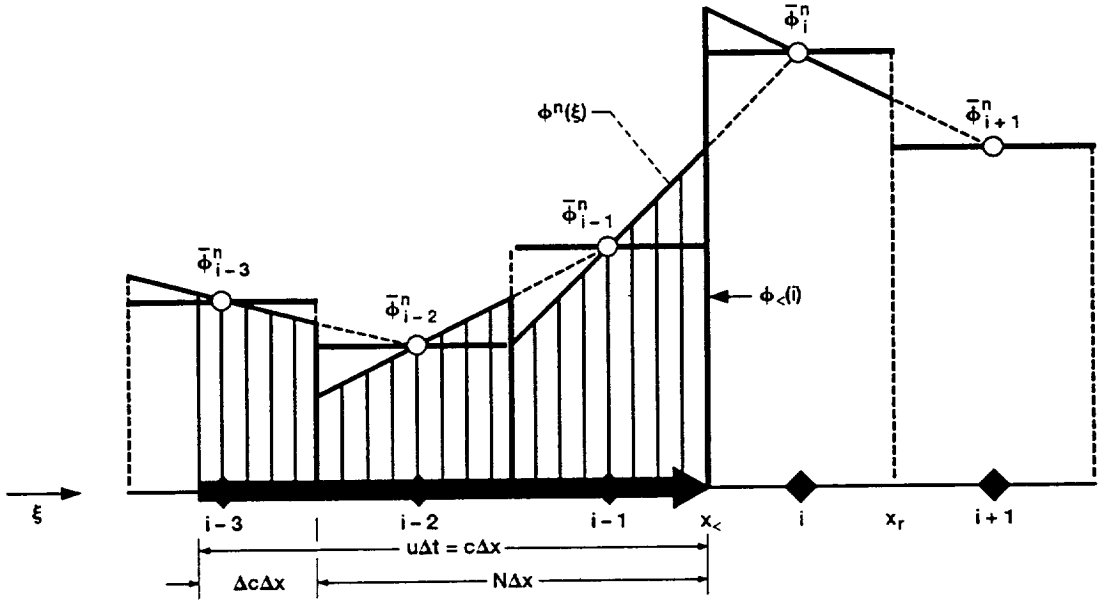

Figure 13.—Large-time-step extension of the Lax-Wendroff scheme, c = 2.625.

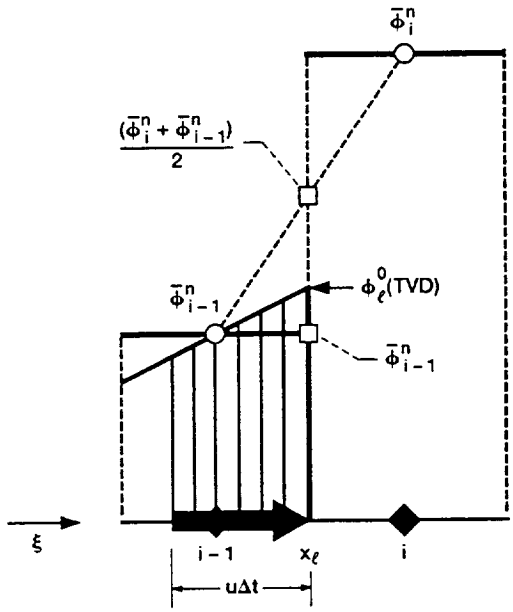

Figure 14.—Definition of ϕ^0_i for TVD constraints, relative to adjacent upstream and downstream cell-average values.

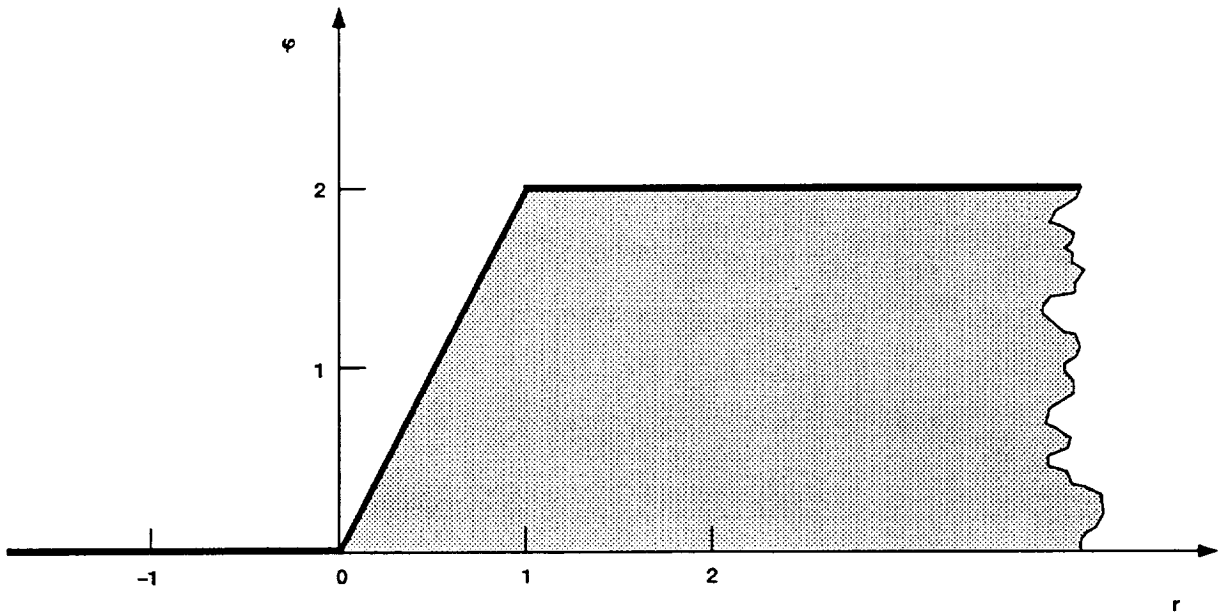

Figure 15.—Sweby's TVD region in (r, φ) coordinates.

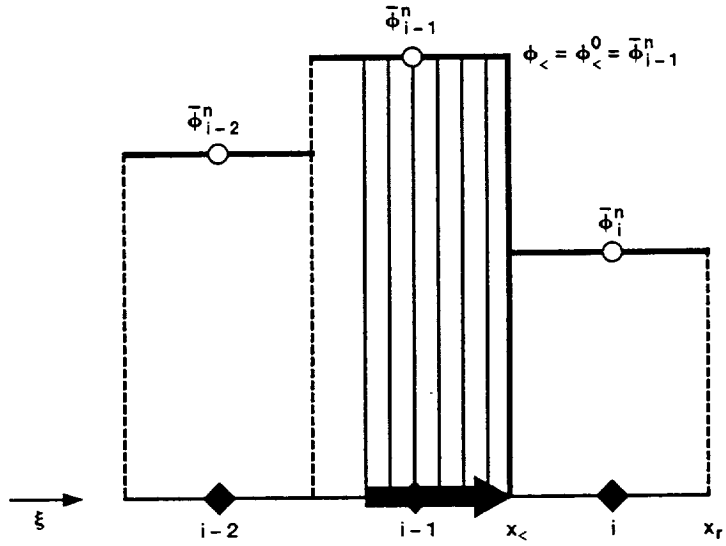

(a) r = -1/2.

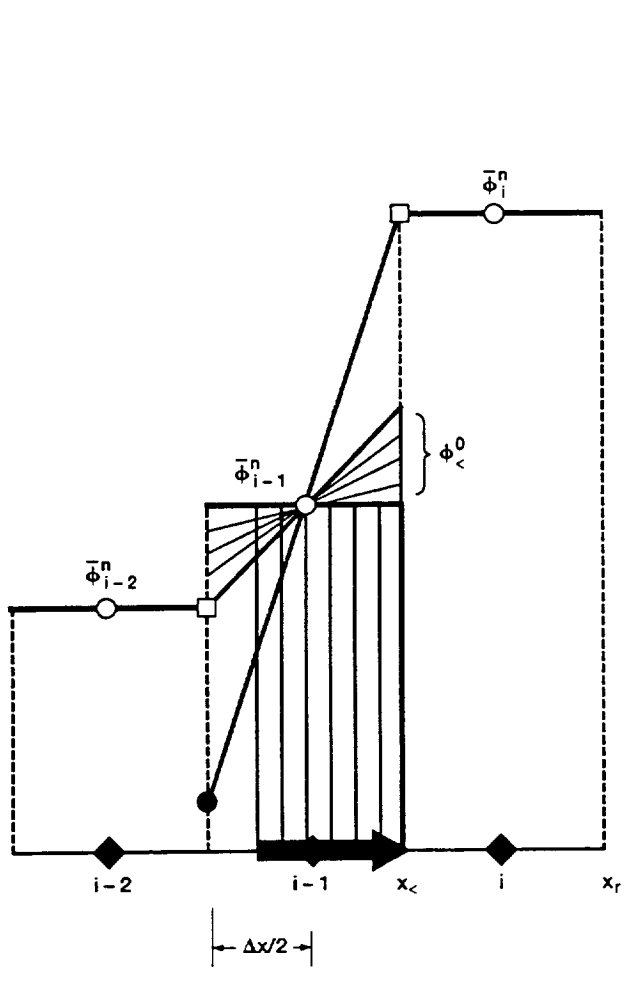

(b) r = 1/3.

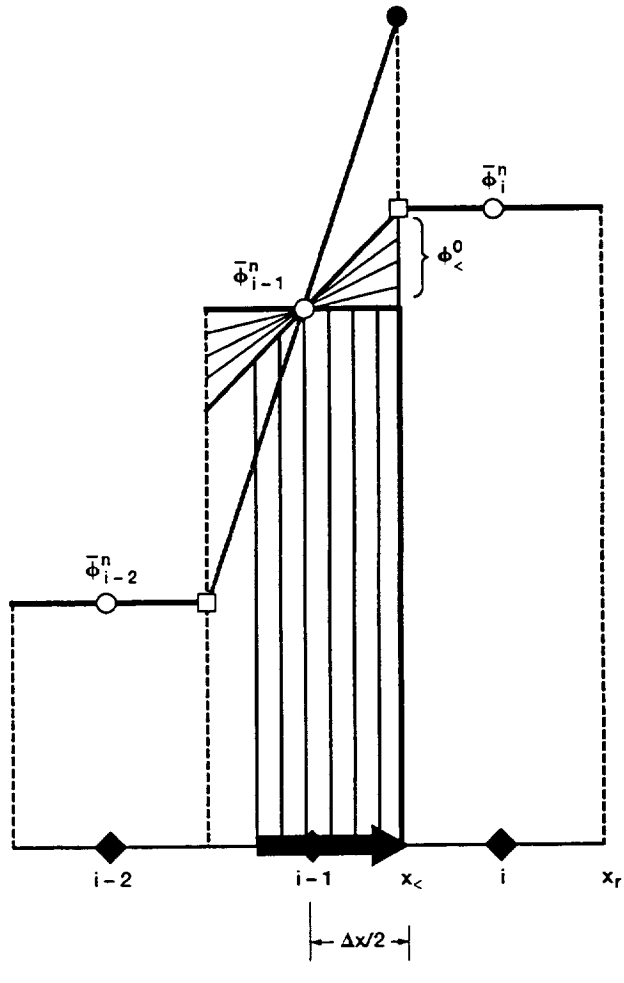

(c) r = 3.

Figure 16.—TVD constraints.

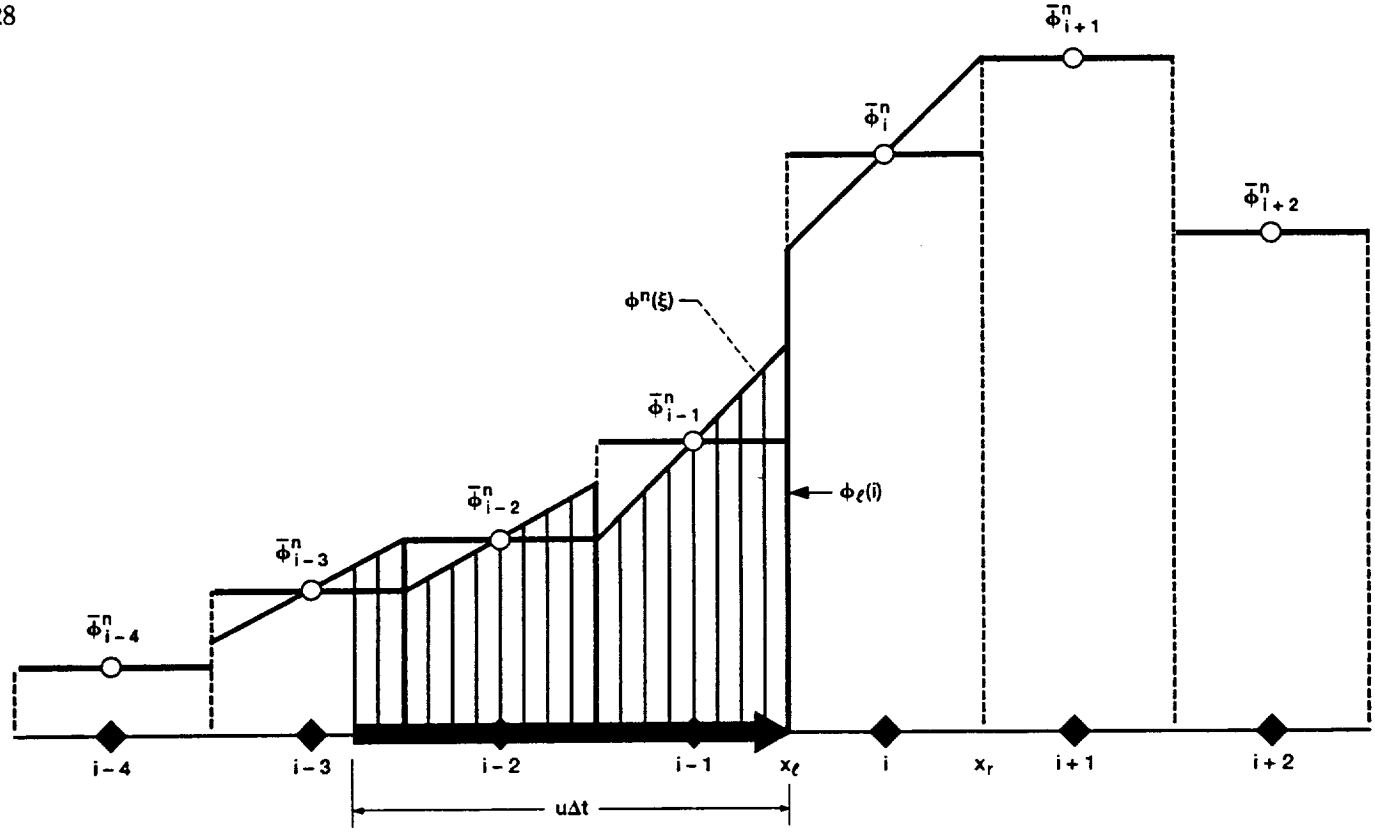

Figure 17.—Large-time-step explicit TVD scheme, c = 2.25.

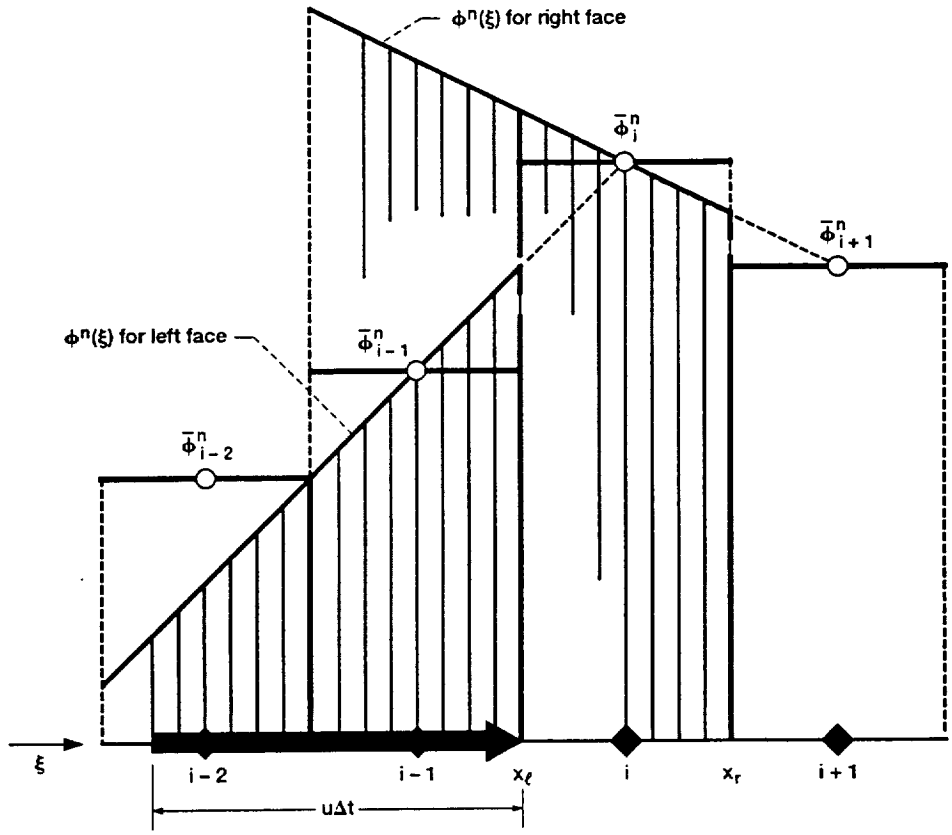

Figure 18.—Conventional Lax-Wendroff sub-grid reconstruction extended beyond its range of validity.

REPORT DOCUMENTATION PAGE

Form Approved
OMB No. 0704-0188

1. AGENCY USE ONLY (*Leave blank*)	2. REPORT DATE	3. REPORT TYPE AND DATES COVERED
	May 1993	Technical Memorandum

4. TITLE AND SUBTITLE

Large Time-Step Stability of Explicit One-Dimensional Advection Schemes

5. FUNDING NUMBERS

WU-505-90-5K

6. AUTHOR(S)

B.P. Leonard

7. PERFORMING ORGANIZATION NAME(S) AND ADDRESS(ES)

National Aeronautics and Space Administration
Lewis Research Center
Cleveland, Ohio 44135-3191

8. PERFORMING ORGANIZATION REPORT NUMBER

E-7867

9. SPONSORING/MONITORING AGENCY NAME(S) AND ADDRESS(ES)

National Aeronautics and Space Administration
Washington, D.C. 20546-0001

10. SPONSORING/MONITORING AGENCY REPORT NUMBER

NASA TM-106203
ICOMP-93-14

11. SUPPLEMENTARY NOTES

B.P. Leonard, Institute for Computational Mechanics in Propulsion, Lewis Research Center, and the University of Akron, Akron, Ohio 44325, (work funded under NASA Cooperative Agreement NCC3-233). ICOMP Program Director, Louis A. Povinelli, (216) 433-5818.

12a. DISTRIBUTION/AVAILABILITY STATEMENT

Unclassified - Unlimited
Subject Category 64

12b. DISTRIBUTION CODE

13. ABSTRACT ***(Maximum 200 words)***

There is a wide-spread belief that most explicit one-dimensional advection schemes need to satisfy the so-called "CFL condition" – that the Courant number, $c = u\Delta t/\Delta x$, must be less than or equal to one, for stability in the von Neumann sense. This puts severe limitations on the time-step in high-speed, fine-grid calculations and is an impetus for the development of implicit schemes, which often require less restrictive time-step conditions for stability, but are more expensive per time-step. However, it turns out that, at least in one dimension, if explicit schemes are formulated in a consistent flux-based conservative finite-volume form, von Neumann stability analysis *does not place any restriction* on the allowable Courant number. Any explicit scheme that is stable for $c < 1$, with a complex amplitude ratio, $\mathbf{G}(c)$, can be easily extended to arbitrarily large c. The complex amplitude ratio is then given by $\exp(-iN\Theta)\,\mathbf{G}(\Delta c)$, where N is the integer part of c, and $\Delta c = c - N\ (< 1)$; this is clearly stable. The CFL condition is, in fact, not a stability condition at all, but, rather, a "range restriction" on the "pieces" in a piece-wise polynomial interpolation. When a global view is taken of the interpolation, the need for a CFL condition evaporates. A number of well-known explicit advection schemes are considered and thus extended to large Δt. The analysis also includes a simple interpretation of (large-Δt) TVD constraints.

14. SUBJECT TERMS

von Neumann stability; Advection schemes; Explicit CFD schemes;
CFL condition; Unconditional stability

15. NUMBER OF PAGES

30

16. PRICE CODE

A03

17. SECURITY CLASSIFICATION OF REPORT	18. SECURITY CLASSIFICATION OF THIS PAGE	19. SECURITY CLASSIFICATION OF ABSTRACT	20. LIMITATION OF ABSTRACT
Unclassified	Unclassified	Unclassified	

National Aeronautics and
Space Administration

Lewis Research Center
ICOMP (M.S. 5-3)
Cleveland, Ohio 44135

FOURTH CLASS MAIL

ADDRESS CORRECTION REQUESTED